ChemistryOPEN Full Papers

ChemPubSoc Europe

Open Access

DOI: 10.1002/open.201402022

Multifunctional Benzothiadiazole-Based Small Molecules Displaying Solvatochromism and Sensing Properties toward Nitroarenes, Anions, and Cations**

María Alfonso, Arturo Espinosa, Alberto Tárraga,* and Pedro Molina*[a]

Aryl or heteroaryl 5-substituted imidazo-benzothiadiazole derivatives were synthesized and shown to display remarkable solvatofluorochromism and selectively sense mercury(II) cations, acetate anions, and nitroaromatic derivatives, with discrimination between *p*-nitrophenol and picric acid. These novel sensors are of importance these days, as the detection of explosives is a high priority in issues of national security and environmental protection. To determine the ion binding properties of the sensors, their absorption and fluorescence emission spectra upon binding different cations and anions were compared. Significant shifts in the spectra were only observed for mercury(II) and acetate. The binding of these two ions was further studied using ^{1}H NMR. The binding properties of different nitroaromatic compounds were also determined, and the results showed the importance of the presence of a phenol group in the guest molecule. Specifically, the two sensors were shown to discriminate between *p*-nitrophenol and picric acid. Finally, the mechanism of fluorescence quenching upon addition of nitrophenols was determined by computational methods.

Introduction

The development of multi-ion-responsive, unimolecular systems has become a challenging task in the field of supramolecular chemistry. In this context, exciting new prospects in the field include molecular logic gates,[1] molecular keypad lock devices,[2] lab-on-molecule type devices,[1a,3] and ion-pair receptors,[4] based on the amphoteric nature of the imidazole ring, which can function as a selective and effective anion and/or cation and even neutral organic molecule receptor system.[5]

On the other hand, organic dyes with intense fluorescence, especially in the solid state,[6] have received considerable attention for their wide applications in optoelectronic materials,[7] biological sensors,[8] and fluorescence imaging.[9] Although a number of organic dyes with strong emission in solution have been reported, in most cases, their fluorescence is quenched in the solid state mainly owing to aggregation and intermolecular interaction. Organic dyes with intense fluorescence in both solution and solid state are still limited. Therefore, the design and synthesis of luminescent materials possessing luminescence in the solid state is very attractive and of great importance.

Benzothiadiazole-derived molecules are widely investigated nowadays due to their well-known photophysical properties, such as a high extinction coefficient, intense fluorescence in both solution and the solid state, and a large Stokes shift.[10]

The design of receptors that contain two different binding sites for the complexation of cationic and anionic guest species is an emerging and topical field of supramolecular chemistry. Due to its amphoteric nature, the imidazole ring can function as a selective and effective anion and/or cation, and even a neutral organic molecule receptor system. In fact, the imidazole ring behaves as an excellent hydrogen-bond donor moiety in synthetic anion receptor systems, and the acidity of the NH proton of the imidazole can be modulated by changing the electronic properties of the imidazole substituents. On the other hand, the presence of a donor pyridine-like nitrogen atom within the ring, capable of selectively binding cationic species, also converts the imidazole derivatives into excellent metal ion sensors.[5]

Detection of explosives is a high priority challenge for life security and health/environmental issues.[11] Among explosive compounds, nitroaromatics are perhaps the most widely used in criminal acts, in landmines, and in cluster bombs. 2,4,6-Trinitrotoluene (TNT) and 2,4-dinitrotoluene (DNT) are the primary constituents of many unexploded landmines worldwide, and picric acid (PA) is very powerful with an explosive power stronger than even TNT.[12,13] Moreover, PA causes several health effects, is a strong irritant to skin, and can cause potential damage to organs involved in the respiratory system.[13] On the other hand, PA has been widely used in pharmaceuticals, dye industries, and as a common reagent in chemical laborato-

[a] *M. Alfonso, Dr. A. Espinosa, Prof. A. Tárraga, Prof. P. Molina*
Departamento de Química Orgánica, Universidad de Murcia
Campus de Espinardo, 30100 Murcia (Spain)
E-mail: pmolina@um.es
atarraga@um.es

[**] *This article is part of the Virtual Special Issue "Molecular Sensors"*

Supporting information for this article is available on the WWW under http://dx.doi.org/10.1002/open.201402022.

ries. Due to its wide use, it can easily contaminate soil and ground water when exposed. Hence development of efficient sensors for the detection of PA is a challenging task for synthetic chemists in order to prevent terrorist threats as well as to detect its presence as an environmental pollutant.

It is worth mentioning here that *p*-nitrophenol derivatives are also among the most toxic pollutants evaluated by US Environmental Protection Agency (EPA).[14] Design and development of chemosensors for rapid and selective detection of nitroaromatic analytes (explosives); in particular, TNT, DNT, and PA, are perceived to be of great importance due to their potential utility in national security screening and also for the environmental concerns.[11b,15] Various methods have been employed for the detection of nitroaromatic compounds; among these, fluorescence sensing is widely employed because of its high sensitivity and quick response. The electron-deficient nature of the aforementioned analytes makes them amenable to detection by electron-rich fluorescence sensors via a photoinduced electron transfer (PET) quenching mechanism.[16] Even though several π-electron-rich fluorescent organic polymers[15c,e,16b,c] and metal–organic architectures[17] have been employed to detect the presence of electron deficient nitroaromatics, development of suitable organic chemosensors with high selectivity for PA is still a very challenging task.[18]

Here, we describe the photophysical and binding properties of multifunctional small-molecules **2** and **3**, which behave as selective fluorescent chemosensors not only for both cations and anions but also for neutral molecules such as nitroaromatic compounds. To this end, we have combined the benzothiadiazole ring with the imidazole ring, which can function as a selective anion and/or cation receptor system. The resulting imidazo-2,1,3-benzothiadiazole, additionally decorated with a pyrrole or triphenylamine unit, displayed either binding or fluorescent properties. Most noteworthy is the multiresponsive character of the imidazo-benzothiadiazole receptors (**2** and **3**) and their ability to act not only as strong fluorescent sensors but also as favorable binding sites for anions, cations and neutral nitroarenes, displaying discrimination in the recognition event towards PA.

Results and Discussion

Target receptors **2** and **3** were prepared in 40% yield from 4,5-diamino-2,1,3-benzothiadiazole **1**[19] by condensation with 2-formylpyrrole and 4-diphenylaminobenzaldehyde, respectively (Scheme 1), and characterized by standard techniques (see Figure S1–S11 in the Supporting Information).

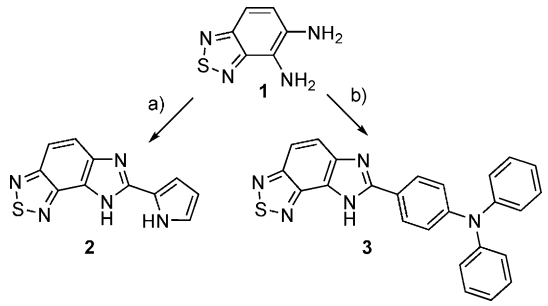

Scheme 1. Synthesis of receptors **2** and **3**. *Reagents and conditions*: a) 2-formylpyrrole, $PhNO_2$, 60 °C; b) 4-(diphenylamino)benzaldehyde, $PhNO_2$, 60 °C; 24 h, 40% (over two steps).

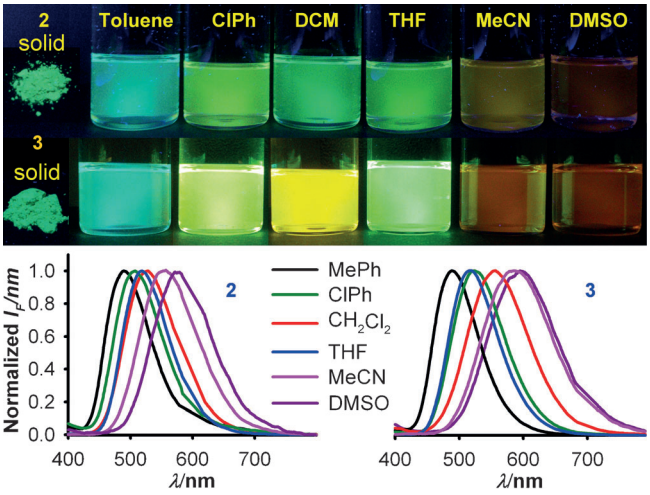

Figure 1. Solvent-dependent emission spectra of **2** (λ_{exc} = 300 nm) and **3** (λ_{exc} = 350 nm) ($c = 10^{-6}$ M). Inset: Visual changes observed in the fluorescence under a UV lamp (λ = 365 nm) in the solid state and in solution of different solvents.

Solvatochromism

Compound **2** is a yellow powder soluble in common organic solvents. Both the powder and the solutions of this receptor in organic solvents give a strong photoluminiscence under irradiation with a general UV lamp (λ = 365 nm) (Figure 1). The solvent polarity has an effect on the emission wavelength of the compound. The maximum emission (λ_{max}) band shifts to a longer wavelength with increase in the polarity of the solvent: for example, from 490 nm in toluene to 575 nm in DMSO, with the Stokes shift varying from 5102 to 7557 cm^{-1}. The same trend was also observed for compound **3** where the magnitude of the red-shift observed in the emission band is also dependent on solvent polarity: from 488 nm in toluene to 595 nm in DMSO (Table 1). This solvatofluorochromism observed for the phospholuminescence suggests that the photoexcited states have a polar nature, which is stabilized by solvation, and the light emission takes place from the stabilized molecules. In contrast, the UV/Vis absorption spectra did not show noticeable solvatochromism, as expected, due to the low polarity of these receptors in their ground states and only a very slight batochromic shift of the λ_{max} was observed by varying the solvent(Table 1 and Figure S13 in the Supporting Information).

Thus, the aforementioned photophysical properties of receptors **2** and **3** revealed that the intense fluorescence, both in solution and solid state, and the large Stokes shift values could be the general properties of substituted imidazo-benzothiadiazoles.

Table 1. UV/Vis and emission data for compounds **2** and **3**.

Compd	Solvent	λ_{max} [nm] (ε)[a]	λ_{em} [nm]	Φ[b]	$\Delta\tilde{\nu}$ [cm^{-1}][c]
2	H_3C-C_6H_5	392 (340)	490	0.280	5102
2	Cl-C_6H_5	391 (340)	510	0.364	5968
2	CH_2Cl_2	385 (420)	525	0.334	6926
2	THF	399 (390)	520	0.286	5832
2	CH_3CN	391 (340)	555	0.115	7557
2	DMSO	405 (320)	575	0.054	7300
3	H_3C-C_6H_5	355 (347)	488	0.232	7677
3	Cl-C_6H_5	357 (342)	525	0.267	8963
3	CH_2Cl_2	355 (392)	555	0.189	10151
3	THF	349 (348)	515	0.244	8990
3	CH_3CN	350 (377)	585	0.031	11477
3	DMSO	355 (368)	595	0.048	11602

[a] UV/Vis data; values in parentheses are ε 10^{-3} in $dm^3 mol^{-1} cm^{-1}$. [b] fluorescence quantum yields. [c] Stokes shift ($\Delta\tilde{\nu}$) calculated as $1/\lambda_{max,abs}$-$1/\lambda_{max,em}$.

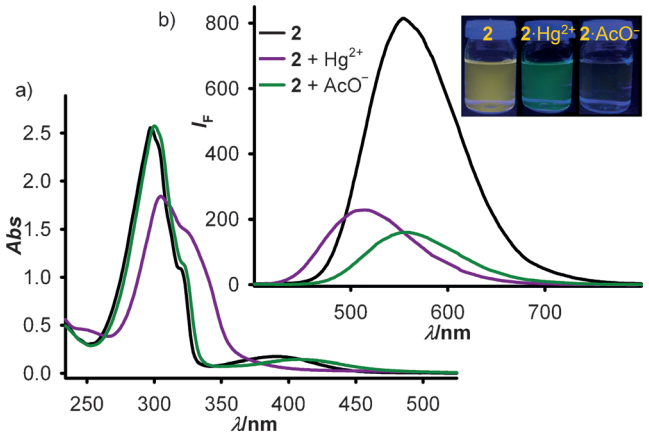

Figure 2. Changes in the absorption spectrum (a) and emission spectrum (b) of **2** (black) in CH_3CN in the presence of $Hg(OTf)_2$ (purple) and $[(nBu)_4N]AcO$ (green). Inset: visual changes observed in the fluorescence of CH_3CN solutions.

Cation and anion binding properties

To investigate the applications of receptors **2** and **3** as chemical sensors for ions, their chemosensory characteristics were investigated towards a number of cations and anions in acetonitrile.[20] In the presence of Hg^{2+} cations, the absorption low-energy band at a λ value of 391 nm disappears with concomitant appearance of a new blue-shifted absorption band at 325 nm. The emission band is blue-shifted from 555 nm to 512 nm ($\Delta\lambda = -43$ nm), and the intensity significantly decreases in the presence of Hg^{2+}. The absorption and emission spectral intensity and wavelength remain almost unchanged in the presence of the other tested cations. The effects of several types of anions were investigated. Only in the presence of AcO^- anions is the low-energy absorption band red-shifted ($\Delta\lambda = 17$ nm), whereas addition of CN^-, $HP_2O_7^{3-}$, and F^- anions clearly induce deprotonation (Figure S14–S16 in the Supporting Information). In addition, a decrease ($I_0/I_F = 5$) of the emission spectral intensity of the receptor was observed in the presence of AcO^- anions, although the wavelength remained unchanged (Figure 2). The stoichiometries of the receptor/guest ion systems were determined using the Job plots obtained from the spectrophotometric titration data (Figure S19 in the Supporting Information), and the results suggest a 1:1 binding (receptor/AcO^- anion), with an association constant[21] (K_a) of $4.45 \times 10^5\ M^{-1}$ and a detection limit[22] of 1.07 $\mu g\ mL^{-1}$. For the case of metal cations, a 2:1 stoichiometric ratio (receptor/cation) was observed, with a K_a value of $1.98 \times 10^9\ M^{-2}$ and a detection limit of 0.13 $\mu g\ mL^{-1}$. The electrospray ionization mass spectrometry (ESI-MS) spectrum of **2** in the presence of Hg^{2+}cations shows a peak at *m/z* 681.2 ($[M^+ - 2H]^-$) indicative of the formation of the 2:1 complex. The relative abundance of the isotopic clusters is also in good agreement with the simulated spectra for such a 2:1 complex (Figure S20–S21 in the Supporting Information).

In case of receptor **3**, the UV/Vis titration upon addition of the set of cations demonstrated that **3** is able to selectively bind to Hg^{2+} metal cations. Thus, the characteristic absorption band at 350 nm gradually decreased upon increasing Hg^{2+} while the simultaneous appearance of a new band centered at a λ value of 367 nm ($\Delta\lambda = 17$ nm) was observed (Figure 3 and Figure S22 in the Supporting Information). Similar to receptor **2**, the intensity of the emission band of **3** decreases upon increasing the amount of Hg^{2+} metal cation ($I_0/I_F = 61$) (Figure 3 and Figure S23 in the Supporting Information). This metal cation formed complexes with a 2:1 stoichiometry (receptor/metal cation), as assessed by the method of continuous variation (Job plot) and ESI-MS (Figure S24–S26 in the Supporting Information). The corresponding calculated K_a value is $2.76 \times 10^8\ M^{-2}$. On the other hand, receptor **3** did not show significant differences in relation to **2** upon addition of anions, and a noticeable selectivity could also be observed towards the acetate anion, when both UV/Vis and fluorescent titrations were carried out (Tables S4 and S5, and Figure S27–S29 in the Supporting Information) in the presence of the set of anions tested. Moreover, the appearance of clear isosbestic points (IP) during the titration processes both with Hg^{2+} metal cation and AcO^-

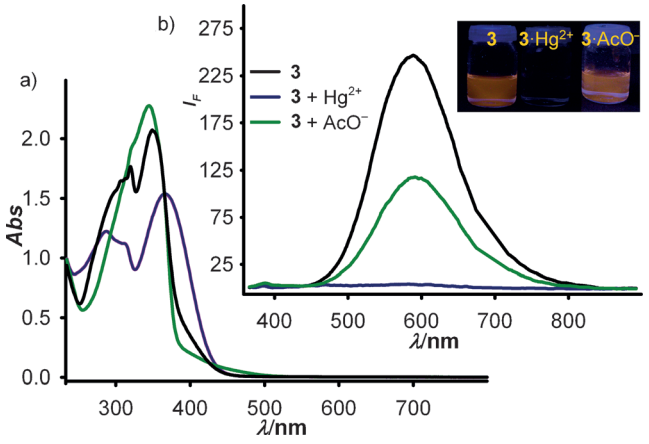

Figure 3. Changes in the absorption spectrum (a) and emission spectrum (b) of **3** (black) in CH_3CN in the presence of $Hg(OTf)_2$ (blue) and $[(nBu)_4N]AcO$ (green). Inset: visual changes observed in the fluorescence of CH_3CN solutions.

anion (Table S4 in the Supporting Information) clearly suggest the generation of two species in the system during the detection processes of both analytes.

The binding properties of **2** and **3** toward Hg^{2+} and AcO^- were also studied by monitoring the ^1H NMR spectral changes caused by the addition of aliquots of these ions to solutions of the receptors in deuterated acetonitrile. The spectral changes observed upon addition of Hg^{2+} to receptor **2** are evident from Figure 4, suggesting that **2** recognizes Hg^{2+} via coordination bond interaction between the N3 and N4 and the metal ion, which induces the general downfield shifts observed in the signals of the receptor during the recognition process (Figure S31 in the Supporting Information). On the other hand, upon addition of AcO^- anion, the signals corresponding to the NH protons collapse into one equivalent signal that was significantly downfield shifted ($\Delta\delta = 2.89$ and $\Delta\delta = 3.81$ ppm) suggesting their binding with the anion through hydrogen-bond interactions. It is also worth mentioning that a very slight upfield shift was also observed for the H7 signal ($\Delta\delta = -0.13$), while signals for H5′, H4′, and H3′ remained almost unaffected (Figure 4 and Figure S32 in the Supporting Information).

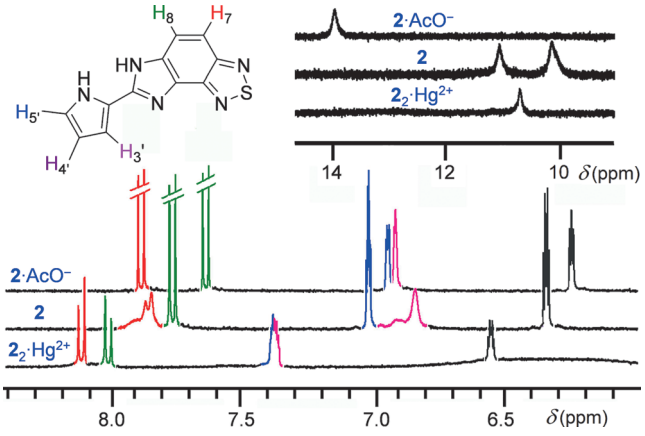

Figure 4. Changes in the ^1H NMR (in CD_3CN) spectrum of **2** (middle) upon addition of [(nBu$_4$N)]AcO (top) and Hg(OTf)$_2$ (bottom).

As shown in Figure 5, the most significant ^1H NMR spectral changes observed upon coordination of Hg^{2+} metal cation to receptor **3** are the following: 1) the H7 and H8 protons within the heterocyclic ring system showed slight downfield shifts ($\Delta\delta = 0.16$ ppm and $\Delta\delta = 0.12$ ppm, respectively); 2) the signals corresponding to the H2′ and H3′ protons, within the *p*-disubstituted phenyl group at the 2-position of the fused imidazole ring, showed a marked upfield shift ($\Delta\delta = -0.30$ ppm and $\Delta\delta = -0.38$ ppm, respectively); 3) while the changes of the *meta* (H3″) and *para* protons (H4″) within the monosubstituted *N*-phenyl rings were not prominent, the signal corresponding to the *ortho* protons (H2″) underwent a very slight upfield shift ($\Delta\delta = -0.14$ ppm) (Table S7 in the Supporting Information). In contrast, addition of AcO^- anion to receptor **3** induce an upfield shift for the signal corresponding to H7 ($\Delta\delta = -0.25$ ppm) while the H8 proton remains almost unaffected ($\Delta\delta = 0.11$ ppm). Simultaneously, the signals corresponding to the *ortho* hydrogen atoms within the phenyl

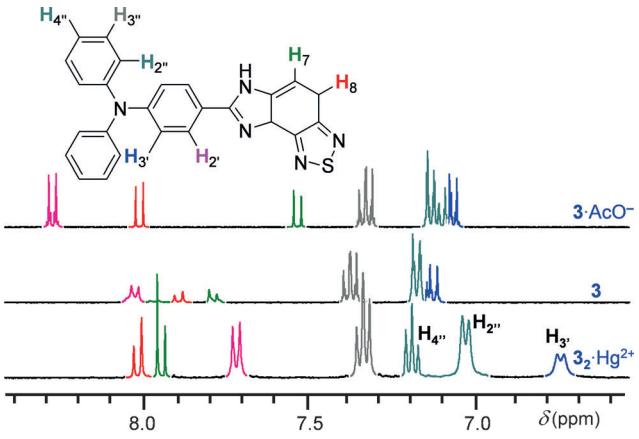

Figure 5. Changes in the ^1H NMR (in CD_3CN) spectrum of **3** (middle) upon addition of Hg(OTf)$_2$ (top) and [(nBu$_4$N)]AcO (bottom).

group at position 5 of the heterocyclic system also showed noticeable downfield shifts in the bound receptor ($\Delta\delta = 0.25$ ppm) (Table S7 in the Supporting Information). Unfortunately, the comparison between the signals of the imidazole NH group in the free and bound receptor could not be estimated because it was impossible to obtain a spectrum due to the limited solubility of this receptor in deuterated acetonitrile.

Detection of aromatics

In order to test the interaction of receptors **2** and **3** with selected nitroaromatic compounds, the following molecules were selected for this study: DNT, 2-nitrotoluene (NT), 2,4-dinitrobenzene (DNB), nitrobenzene (NB), 4-nitrophenol (NP), 2,4-dinitrophenol (DNP) and picric acid (PA). The fluorescence attenuation of receptor **2** in acetonitrile was investigated as the degree of fluorescence quenching response depends on the electron deficiency. While insignificant quenching was observed for NB ($I_0/I_F = 4$), and moderate quenching for DNT, NT, and DNB ($I_0/I_F = 9$), highly efficient quenching was observed for hydroxy-substituted nitroarenes: NP ($I_0/I_F = 50$) and DNP ($I_0/I_F = 20$). Significantly, receptor **2** showed a different sensitivity towards PA because not only was a decrease of the emission band observed ($I_0/I_F = 3$), but also, more importantly, a blue-shift of the wavelength ($\Delta\lambda = -15$ nm) (Figure 6).

A similar picture emerged from the comparison of the emission spectra obtained upon addition of the aforementioned nitroaromatic derivatives to receptor **3**, where the same quenching effect was observed although to a lesser extent. In contrast, addition of PA to **3** resulted in the quenching of its fluorescence but without promoting any shift of its emission wavelength, as receptor **2** did under similar conditions (Figure S36 and S39 in the Supporting Information).

Fluorogenic titrations of receptors **2** and **3** with PA indicated the formation of 1:1 complexes in both cases (Figure S42 in the Supporting Information), with K_a values of $8.2 \times 10^3\ M^{-1}$ for **2** and $4.49 \times 10^3\ M^{-1}$ for **3**, while the detection limits were 159 $\mu g\,mL^{-1}$ and 317 $\mu g\,mL^{-1}$ for **2** and **3**, respectively. Nonaromatic analytes, such as nitromethane, do not give rise to a quenching response due to the lack of π–π interactions.

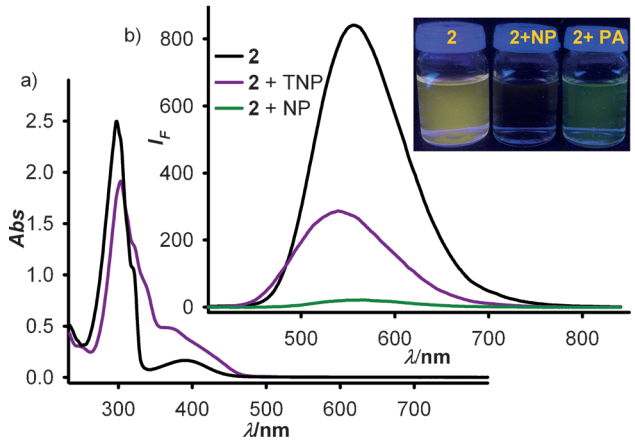

Figure 6. Changes in the absorption spectrum (a) and emission spectrum (b) of **2** (black) in CH_3CN in the presence of picric acid (PA) (purple) and in the presence of *p*-nitrophenol (NP) (green). Inset: visual changes observed in the fluorescence of CH_3CN solutions.

In order to study the behavior of **2** and **3** toward PA, comparison experiments of ^{1}H NMR titration of **2** and **3** with HBF_4 and PA were carried out. As shown in Figure 7, the most significant ^{1}H NMR spectral changes observed in receptor **2** upon addition of HBF_4 and PA were the marked downfield shifts for all the proton signals with respect to those found in the free receptor. However, the magnitudes of the observed changes in chemical shifts ($\Delta\delta$) for those signals were significantly different (Table S11 in the Supporting Information). Moreover, the values of such $\Delta\delta$ promoted by PA were lower than those resulting from the protonation by the HBF_4.

All these results suggest that the presence of a phenol group in the guest molecule is important, because the hydroxy unit forms hydrogen-bonding interactions with the nitrogen atoms in the receptor. Such a ground-state complexation facilitates the fluorescence quenching process. The roles of the nitro groups on the benzene ring are twofold; they affect the electron deficiency of the π system and control the strength (acidity) of the phenol unit for hydrogen bonding. In the case of PA, three nitro groups result in the most deficient π system for driving the fluorescence quenching and the strongest interaction with the nitrogen atoms for promoting the quenching process. As a result, the receptor exhibits an unusual sensitivity and selectivity in response to PA. Thus, in accordance with the ^{1}H NMR data, we believe that the recognition event probably involves an initial proton transfer followed by hydrogen-bond formation and subsequent phenoxide coordination by forming N^+—H···TNP^- hydrogen bonds.[23] In other words, the increasing quenching efficiency with increasing acidity of the phenolic analytes, and the shifts in emission maxima upon addition of PA suggest the presence of electrostatic interactions between PA and the receptor, which are absent in other nitro analytes.

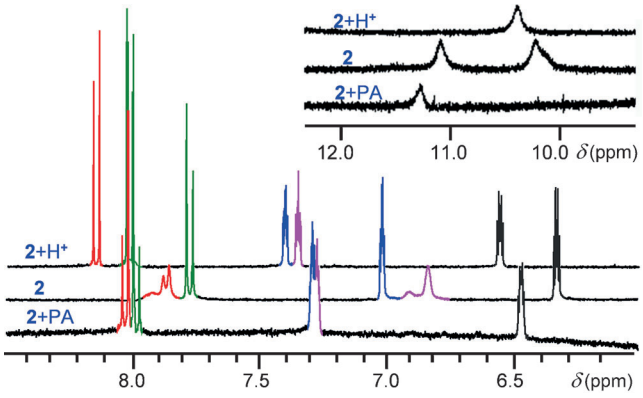

Figure 7. Changes in the ^{1}H NMR (in CD_3CN) spectrum of **2** upon addition of HBF_4 (top) and picric acid (PA) (bottom).

Similarly, addition of HBF_4 and PA to receptor **3** also induced different ^{1}H NMR spectral changes. Thus, upon addition of HBF_4, significant downfield shifts were observed for the H7 and H8 protons within the heterocyclic framework as well as for the protons present in the monosubstituted N-phenyl rings. Moreover, the doublet corresponding to the H2′ aromatic protons of the *p*-disubstituted phenyl group were significantly upfield shifted, while the doublet associated to the H3′ protons was almost unaffected. The changes promoted by PA are clearly illustrated in Figure 8. Although the shifts in the proton signals induced by PA with respect to those observed in the free receptor followed the same trend as those found upon addition of HBF_4, the magnitudes of the resulting upfield or downfield shifts were considerably different (Table S12 in the Supporting Information). Therefore, the phenomena involved in this recognition process should be almost similar to the aforementioned case of receptor **2**.

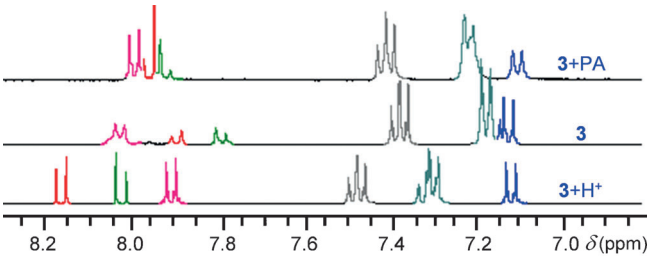

Figure 8. Changes in the ^{1}H NMR (in CD_3CN) spectrum of **3** upon addition of picric acid (PA) (top) and HBF_4 (bottom).

Theoretical calculations

In order to obtain some additional information regarding the mechanism of fluorescence quenching in **2** upon addition of nitrophenols, the simplest reaction with NP was modeled computationally. An initial acid–base reaction (see above) must proceed by protonation of **2** at the basic imidazole N6 atom, resulting in a **2**·H^+ species that is more stable than those protonated at the thiadiazole N3 and N1 atoms by 13.58 and 13.40 kcal mol^{-1}, respectively, at the optimization level. The overall transformation of **2** and NP into the isolated conjugated acid/base species **2**·H^+ and 4-nitrophenolate is remarkably endergonic by 21.19 kcal mol^{-1} at the $COSMO_{MeCN}$/DLPNO-CCSD(T)/def2-TZVP level. Nevertheless, previous π-stacking between the reagents favors the proton-transfer process due to occurrence of three simultaneous noncovalent interactions (NCIs): namely the electrostatic attraction between cation and

anion within the ion pair $[\mathbf{2}\cdot H]^+\cdot[4\text{-}O_2N\text{-}C_6H_4\text{-}O]^-$, strong hydrogen bonding between the pyrrolic NH and the phenolate O atom ($d_{O\cdots H}=1.754$ Å; WBI = 0.063; LBO = 0.241; $\rho(r)=4.07\times10^{-2}$ e/a_o^3), and the resulting tight π-stacking characterized by three bond critical points (BCP) ($\Sigma\rho(r)=2.52\times10^{-2}$ e/a_o^3). These NCIs are conveniently visualized by reduced electron density (RDG) isosurfaces using the NCIplot technique (Figure 9).[24,25]

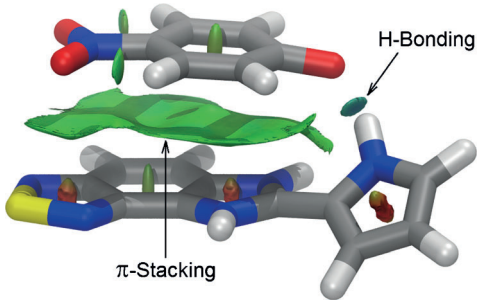

Figure 9. Computed (M06-2X/def2-TZVP-f) most stable structure for ion pair $[\mathbf{2}\cdot H]^+\cdot[4\text{—}O_2N\text{—}C_6H_4\text{—}O]^-$ with NCIplot highlighting key stabilizing noncovalent interactions (NCIs). The RDG $s=0.5$ au isosurface is colored over the range $-0.07<\text{sign}(\lambda_2)\cdot\rho<0.07$ au: blue denotes strong attraction, green stands for moderate interaction, and red indicates strong repulsion.

The mean planes of both ionic components are almost parallel ($\measuredangle=1.7°$) and located at a rather short distance of 3.159 Å (average of orthogonal distances of the centroid of one ring system into the mean plane of the other). The phenoxide C–O bond is slightly bent inwards and the pyrrolyl substituent rotated (NCCN dihedral $\measuredangle=36.7°$) to enable for hydrogen-bond formation. At the working DLPNO-CCSD(T) level of theory, formation of the ion pair was found to be only slightly endergonic from the isolated reagents by 7.17 kcal mol^{-1}, and it is believed to account for deactivation of the intrinsic fluorescence of the receptor; a phenoxide-centered HOMO is located energetically between the receptor-centered orbitals involved in fluorescence HOMO-1 and LUMO (see the Supporting Information). A good agreement was found for the ion-pair formation energy computed with the same basis set and solvation model at lower levels such as SCS-MP2 (8.62 kcal mol^{-1}) and LPNO-NCEPA/1 (0.76 kcal mol^{-1} lower than the highest reference level, before BSSE correction; see Computational Methods in the Experimental Section), whereas only M06-2X (3.82 kcal mol^{-1}) and Grimme's PWBP95-D3 level (2.67 kcal mol^{-1}) predict a rather thermoneutral balance.

Conclusions

We have developed two heteroditopic receptors **2** and **3**, which display solvatofluorochromism and behave as true "lab-on-a-molecule" probes. They have been shown to be selective dual channel chemosensors for mercury (II) and acetate ions. Interestingly, both receptors act as luminescent molecular chemosensors for the detection of nitroaromatic compounds, particularly exhibiting selective response towards picric acid.

Experimental Section

Chemistry

General Remarks: Melting points were determined on a hot-plate melting point apparatus and are uncorrected. ^{1}H and ^{13}C NMR spectra were recorded at 300 and 75 MHz, respectively, for **2**, and 400 and 100 MHz, respectively, for **3**. HMBC and HMQC spectra were recorded at 400 MHz. Chemical shifts (δ) are given relative to the signals of tetramethylsilane in the case of ^{1}H and ^{13}C spectra. UV/Vis spectra were obtained using a UV/Vis near infrared spectrophotometer with a dissolution cell path of 10 mm. The samples were dissolved in CH_3CN ($c=5\times10^{-5}$ M), and the spectra were recorded with the spectra background corrected before and after the sequential additions of aliquots of 0.1 equiv of cations or anions in CH_3CN ($c=2.5\times10^{-2}$ M) and aliquots of 10 equiv of nitroarenes in CH_3CN ($c=0.5$ M). Fluorescence spectra were carried out in a fluorescence spectrophotometer using a fluorescence cell of 10 mm ($c=5\times10^{-6}$ M for **2** and 1×10^{-5} M for **3** in CH_3CN). Before recording the spectra, the samples were deoxygenated, to remove fluorescence quenching via oxygen, by bubbling nitrogen through the solution for at least 10 min. All spectra were recorded before and after the sequential additions of aliquots of 0.1 equiv of a solution of cations or anions in CH_3CN ($c=3\times10^{-3}$ M for **2** and 6×10^{-3} M for **3**) and aliquots of 10 equiv of nitroarenes in CH_3CN ($c=0.3$ M for **2** and 0.6 M for **3**). Quantum yield values were measured with respect to anthracene as standard ($\Phi=0.27\pm0.01$),[26] using the equation $\Phi_x/\Phi_s=(S_x/S_s)[(1-10^{-As})/(1-10^{-Ax})]^2(n_s^2/n_x^2)$ where x and s indicate the unknown and standard solution, respectively, Φ is the quantum yield, S is the area under the emission curve, A is the absorbance at the excitation wavelength, and n is the index of refraction. The recognition properties were investigated in the presence of several metal cations (Li^+, Na^+, K^+, Ca^{2+}, Mg^{2+}, Cd^{2+}, Cu^{2+}, Ni^{2+}, Zn^{2+}, Pb^{2+}, and Hg^{2+}) and anions (F^-, Cl^-, Br^-,I^-, $H_2PO_4^-$, $HP_2O_7^{3-}$, HSO_4^-, CN^-, AcO^-, PF_6^-, BF_4^-, ClO_4^-, NO_3^-, and OH^-).[20]

General procedure for the preparation of 5-substituted-6*H*-imidazo[4,5-*e*]-2,1,3-benzothiadiazoles 2 and 3: To a solution of the appropriate aldehyde (1.72 mmol) in nitrobenzene (12 mL) and acetic acid (0.5 mL), 4,5-diamino-2,1,3-benzothiadiazole (0.29 g, 1.72 mmol) was added. The reaction mixture was stirred for 24 h at 60 °C. Afterwards, a saturated aq solution of $NaHCO_3$ was added until pH 7 was achieved. The resulting mixture was poured into water (50 mL) and extracted with CH_2Cl_2 (2×50 mL). The combined organic phase was dried over anhyd $NaSO_4$, filtered and concentrated under vacuum. The resulting residue was chromatographed on a silica gel column twice, first using CH_2Cl_2/Et_2O (7:3), and then using CH_2Cl_2/MeOH (9.5:0.5). Finally, recrystallization from CH_2Cl_2 gave the desired compound as a yellow solid.

5-(2-Pyrrolyl)-6*H*-imidazo[4,5-*e*]-2,1,3-benzothiadiazole (2): Yield = 40 % (0.16 g); mp: 260–264 °C (decomp); ^{1}H NMR (300 MHz, CD_3OD, Me_4Si): $\delta_H=6.28$ (1 H, dd, $J_{3',4'}$ 3.6; $J_{4',5'}$ 2.7, $H_{4'}$); 6.89 (1 H, dd, $J_{3',5'}$ 1.2; $J_{3',4'}$ 3.6, $H_{3'}$); 7.01 (1 H, dd, $J_{3',5'}$ 1.2, $J_{4',5'}$ 2.7, $H_{5'}$); 7.73 (1 H, d, $J_{7,8}$ 9.3, H_8); 7.82 ppm (1 H, d, $J_{7,8}$ 9.3, H_7); ^{13}C NMR (100 MHz, CD_3OD, Me_4Si): $\delta_C=110.7$ ($C_{3'}$, $C_{5'}$), 116.5 (C_7, C_8), 122.6 ($C_{5'}$), 122.9 ($C_{2'}$), 147.9 (C_5), 155.1 ppm (C_{8a}); HRMS-ESI: $[M+1]$ m/z calcd for $C_{11}H_7N_5S$: 242.0495, found: 242.0504.

5-[4-(*N*,*N*-Diphenyl)aminophenyl]-6*H*-imidazo[4,5-*e*]-2,1,3-benzothiadiazole (3): Yield = 40 % (0.288 g); mp: 275–277 °C (decomp); ^{1}H NMR (400 MHz, [D$_6$]DMSO, Me_4Si): $\delta_H=7.07$ (d, 2 H, $J_{2',3'}=8.8$ Hz, $H_{3'}$), 7.12 (m, 6 H, $H_{2''}+H_{4''}$), 7.36 (m, 4 H, $H_{3''}$), 7.78 (d, 1 H, $J_{7,8}=9.2$ Hz, H_7), 7.93 (d, 1 H, $J_{7,8}=9.2$ Hz, H_8), 8.11 (d, 2 H, $J_{2',3'}=8.8$ Hz,

$H_{2'}$), 13.58 ppm (br s, 1H, NH); ^{13}C NMR (100 MHz, CD_3OD, Me_4Si): $\delta_C = 116.4$ (C_7), 123.0 ($C_{3'}$), 124.3 ($C_{4'}$), 125.3 ($C_{2'}$, $C_{4'}$), 126.3 ($C_{2''}$, $C_{4'}$), 128.9 ($C_{2'}$), 131.1 ($C_{3''}$); 148.0 ($C_{1''}$), 150.1 (q), 152.1 (q), 154.7 ppm (q); HRMS-ESI: $[M+1]$ m/z calcd for $C_{25}H_{17}N_5S$: 420.1277, found: 420.1283.

Computational methods

Density functional theory (DFT) calculations were performed with the ORCA program.[27] All geometry optimizations were run in redundant internal coordinates using the Truhlar's M06–2X functional[28] together with the def2-TZVP basis set[29] and the new efficient RIJCOSX algorithm.[30] Solvent effects (acetonitrile) were taken into account via the COSMO solvation method.[31] From these optimized geometries, all reported data were obtained by means of single-point (SP) calculations using the more flexible and polarized def2-TZVPP[32] basis set. Unless otherwise stated, all reported energies were obtained using the recently developed near-linear scaling domain-based local pair natural orbital (DLPNO) method[33] to achieve coupled cluster theory with single-double and perturbative triple excitations (CCSD(T)) calculations and were corrected for the zero-point vibrational term at the optimization level. For comparative purposes, energies were also computed using the double-hybrid-*meta*-GGA functional PWPB95[34] together with the latest Grimme's semiempirical atom-pair-wise correction (DFT-D3 methods) accounting for the major part of the contribution of dispersion forces to the energy[35] and spin-component scaled second-order Möller–Plesset perturbation theory (SCS-MP2).[36] Also, LPNO schemes for high-level single-reference methods, such as the coupled electron-pair approximation (CEPA);[37] here the slightly modified NCEPA/1 version[38] implemented in ORCA was used. The energy balance for the formation of the ion pair includes the correction for the basis set superposition error (BSSE), except at the LPNO-NCEPA/1 level, due to convergence problems in the coupled-pair iterations. Wiberg bond indices (WBI) and Löwdin bond orders (LBO) were obtained from the natural bond orbital (NBO)[39] and Löwdin[40] population analyses, respectively. Bader's AIM-derived topological analysis of the electron density[41] was conducted with AIM2000.[42] The electron density computed for the ion pair $[\mathbf{2}\cdot H]^+\cdot[4-O_2N-C_6H_4-O]^-$ with the lower def2-TZVP(-f) basis set was used as input for the NCIplot program. Figure 9 was prepared using VMD–Visual Molecular Dynamics.[43]

Acknowledgements

The authors gratefully acknowledge the financial support from Spanish Ministry of Science and Innovation (MICINN) (Project CTQ2011–27175), Fondo Europeo de Desarrollo Regional (FEDER). M.A., thanks the MICINN for an FPI fellowship.

Keywords: anions · cations · nitroarenes · sensors · solvatochromism

[1] a) D. C. Magri, G. J. Brown, G. D. McClean, A. P. De Siva, *J. Am. Chem. Soc.* **2006**, *128*, 4950 – 4951; b) A. P. De Silva, S. S. K. De Silva, N. C. W. Goonesekera, H. Q. N. Gunaratne, P. L. M. Lynch, K. R. Nesbitt, S. T. Patuwathavithana, L. D. S. Ramyalal, *J. Am. Chem. Soc.* **2007**, *129*, 3050 – 3051; c) U. Pischel, *Angew. Chem. Int. Ed.* **2007**, *46*, 4026 – 4040; *Angew. Chem.* **2007**, *119*, 4100 – 4115; d) S. Kou, H. N. Lee, D. Van Noort, K. M. K. Swamy, S. H. Kim, J. H. Soh, K-M. Lee, S.-W. Nnam, J. Yoon, S. Park, *Angew. Chem. Int. Ed.* **2008**, *47*, 872 – 876; *Angew. Chem.* **2008**, *120*, 886 – 890.

[2] a) M. Kumar, R. Kumar, V. Bhalla, *Chem. Commun.* **2009**, 7384 – 7386; b) D. Margulies, C. E. Felder, G. Melman, A. Shanzer, *J. Am. Chem. Soc.* **2007**, *129*, 347 – 354; c) M. Suresh, A. Ghosh, A. Das, *Chem. Commun.* **2008**, 3906 – 3908.

[3] a) V. Bhalla, V. Vij, M. Kumar, P. R. Sharma, T. Kaur, *Org. Lett.* **2012**, *14*, 1012 – 1015; b) M. Schmittel, H.-W. Li, *Angew. Chem. Int. Ed.* **2007**, *46*, 893 – 896; *Angew. Chem.* **2007**, *119*, 911 – 914.

[4] a) M. Alfonso, A. Tárraga, P. Molina, *Inorg. Chem.* **2013**, *52*, 7487 – 7596; b) P. Molina, A. Tárraga, M. Alfonso, *Dalton Trans.* **2014**, *43*, 18 – 29; c) M. C. González, F. Otón, A. Espinosa, A. Tárraga, P. Molina, *Chem. Commun.* **2013**, *49*, 9633 – 9635; d) F. Otón, M. C. González, A. Espinosa, C. Ramírez de Arellano, A. Tárraga, P. Molina, *J. Org. Chem.* **2012**, *77*, 10083 – 10092; e) M. Alfonso, A. Espinosa, A. Tárraga, P. Molina, *Chem. Commun.* **2012**, *48*, 6848 – 6850; f) M. Alfonso, A. Espinosa, A. Tárraga, P. Molina, *Org. Lett.* **2011**, *13*, 2078 – 2081; g) M. Alfonso, A. Tárraga, P. Molina, *Org. Lett.* **2011**, *13*, 6432 – 6435.

[5] P. Molina, A. Tárraga, F. Otón, *Org. Biomol. Chem.* **2012**, *10*, 1711 – 1724.

[6] a) C.-H. Zhao, Y.-H. Zhao, H. Pan, G.-L. Fu, *Chem. Commun.* **2011**, *47*, 5518 – 5520; b) D. Zhang, Y. Wen, Y. Xiao, G. Yu, Y. Liu, X. Qian, *Chem. Commun.* **2008**, 4777 – 4779; c) M.-J. Lin, A. J. Jimenez, C. Burschka, F. Wurthner, *Chem. Commun.* **2012**, *48*, 12050 – 12052; d) M. Shimizu, Y. Takeda, M. Higashi, T. Hiyama, *Angew. Chem. Int. Ed.* **2009**, *48*, 3653; *Angew. Chem.* **2009**, *121*, 3707; e) Z. Zhang, B. Xu, J. Su, L. Shen, Y. Xie, H. Tian, *Angew. Chem. Int. Ed.* **2011**, *50*, 11654 – 11657; *Angew. Chem.* **2011**, *123*, 11858 – 11861; <lit *f*> C.-H. Zhao, A. Wakamiya, Y. Inukai, S. Yamaguchi, *J. Am. Chem. Soc.* **2006**, *128*, 15934 – 15935; g) C. Yuan, S. Saito, C. Camacho, S. Irle, I. Hisaki, S. Yamaguchi, *J. Am. Chem. Soc.* **2013**, *135*, 8842 – 8845; h) A. Wakamiya, K. Mori, S. Yamaguchi, *Angew. Chem. Int. Ed.* **2007**, *46*, 4273 – 4276; *Angew. Chem.* **2007**, *119*, 4351 – 4354; i) X. Feng, J.-Y. Hu, F. Iwanaga, N. Seto, C. Redshaw, M. R. J. Elsegood, T. Yamato, *Org. Lett.* **2013**, *15*, 1318 – 1321; j) D. Zhao, J. Hu, N. Wu, X. Huang, X. Qin, J. Lan, J. You, *Org. Lett.* **2011**, *13*, 6516 – 6519.

[7] a) T. P. I. Saragi, T. Spehr, A. Siebert, T. Fuhrmann-Lieker, J. Salbeck, *Chem. Rev.* **2007**, *107*, 1011 – 1065; b) Y. S. Zhao, H. Fu, A. Peng, Y. Ma, Q. Liao, J. Yao, *Acc. Chem. Res.* **2010**, *43*, 409 – 418; c) Y. Zhou, J. W. Kim, R. Nandhakumar, M. J. Kim, E. Cho, Y. S. Kim, Y. H. Jang, C. Lee, S. Han, K. M. Kim, J-J. Kim, J. Yoon, *Chem. Commun.* **2010**, *46*, 6512 – 6514; d) Y. Zhou, J. W. Kim, M. J. Kim, W.-J. Son, S. J. Han, H. N. Kim, S. Han, Y. Kim, C. Lee, S.-J. Kim, D. H. Kim, J-J. Kim, J. Yoon, *Org. Lett.* **2010**, *12*, 1272 – 1275; e) T. Qin, W. Wiedemair, S. Nau, R. Trattnig, S. Sax, S. Winkler, A. Vollmer, N. Koch, M. Baumgarten, E. J. W. List, K. Müllen, *J. Am. Chem. Soc.* **2011**, *133*, 1301 – 1303; f) W. Z. Yuan, Y. Gong, S. Chen, X. Y. Shen, J. W. Y. Lam, P. Lu, Y. Lu, Z. Wan, R. Hu, N. Xie, H. S. Kwok, Y. Zhang, J. Z. Sun, B. Z. Tang, *Chem. Mater.* **2012**, *24*, 1518 – 1528; g) C. Li, H. Wonneberger, *Adv. Mater.* **2012**, *24*, 613 – 636; h) S. Schmidbauer, A. Hohenleutner, B. König, *Adv. Mater.* **2013**, *25*, 2114 – 2129.

[8] a) L. Yuan, W. Lin, K. Zheng, L. He, W. Huang, *Chem. Soc. Rev.* **2013**, *42*, 622 – 661; b) L. Wang, Y. Xiao, W. Tian, L. Deng, *J. Am. Chem. Soc.* **2013**, *135*, 2903 – 2906.

[9] a) M. Li, H.-Y. Lu, R.-L. Liu, J.-D. Chen, C.-F. Chen, *J. Org. Chem.* **2012**, *77*, 3670 – 3673; b) H. J. Kim, C. H. Heo, H. M. Kim, *J. Am. Chem. Soc.* **2013**, *135*, 17969 – 17977; <lit *c*> W. Sun, J. Fan, C. Hu, J. Cao, H. Zhang, X. Xiong, J. Wang, S. Cui, S. Sun, X. Peng, *Chem. Commun.* **2013**, *49*, 3890 – 3892.

[10] a) X. Zhang, R. Yamaguchi, K. Moriyama, M. Kadowaki, T. Kobayashi, T. Ishi-i, T. Thierman, S. Mataka, *J. Mater. Chem.* **2006**, *16*, 736 – 740; b) S.-i. Kato, T. Matsumoto, T. Ishi-i, T. Thierman, M. Shigeiva, H. Gorohmaru, S. Maeda, Y. Yamashita, S. Mataka, *Chem. Commun.* **2004**, 2342 – 2343; c) S.-i. Kato, T. Matsumoto, M. Shigeiwa, H. Gorohmaru, S. Maeda, T. Ishi-I, S. Makata, *Chem. Eur. J.* **2006**, *12*, 2303 – 2317; d) Y.-H. Chen, L.-Y. Lin, C.-W. Lu, F. Lin, Z.-Y. Huang, H.-W. Lin, P.-H. Wang, Y.-H. Liu, K.-T. Wong, J. Weng, D. J. Miller, S. B. Darling, *J. Am. Chem. Soc.* **2012**, *134*, 13616 – 13623.

[11] a) Y. Salinas, R. Martinez-Mañez, M. D. Marcos, F. Sancenon, A. M. Costero, M. Parra, S. Gil, *Chem. Soc. Rev.* **2012**, *41*, 1261 – 1296; b) M. E. Germain, M. J. Knapp, *Chem. Soc. Rev.* **2009**, *38*, 2543 – 2555; c) J. Akhavan, *Chemistry of Explosives, 2nd ed.*, Royal Society of Chemistry, London, **2004**; d) J. T. Hamrick, R. C. Va, United States Patent 3515604, **1970**; e) M. Hissler, W. B. Connick, D. K. Geiger, J. E. McGarrah, D. Lipa, R. J. Lachicotte, R. Eisenberg, *Inorg. Chem.* **2000**, *39*, 447 – 457; f) R. Ziessel, H.

Hissler, A. El-ghayoury, A. Harriman, *Coord. Chem. Rev.* **1998**, *178*, 1251 – 1298.
[12] a) J. S. Yang, T. M. Swager, *J. Am. Chem. Soc.* **1998**, *120*, 11864 – 11864; b) S. Shanmugaraju, H. Jadhav, Y. P. Patil, P. S. Mukherjee, *Inorg. Chem.* **2012**, *51*, 13072 – 13074; c) V. W-W. Yam, C.-H. Tao, L. Zhang, K. M.-C. Wong, K.-K. Cheung, *Organometallics* **2001**, *20*, 453 – 459.
[13] B. Roy, A. K. Bar, B. Gole, P. S. Mukherjee, *J. Org. Chem.* **2013**, *78*, 1306 – 1310.
[14] 4-Nitrophenol, Health and Environmental Effects Profile, No. 135, US Environmental Protection Agency, Washington, DC, **1980**.
[15] a) D. T. McQuade, A. E. Pullen, T. M. Swager, *Chem. Rev.* **2000**, *100*, 2537 – 2574; b) K. J. Albert, N. S. Lewis, C. L. Schauer, G. A. Sotzing, S. E. Stizel, T. P. Vaid, D. R. Walt, *Chem. Rev.* **2000**, *100*, 2595 – 2626; c) H. Sohn, R. M. Calhoun, M. J. Sailor, W. C. Trogler, *Angew. Chem. Int. Ed.* **2001**, *40*, 2104 – 2105; *Angew. Chem.* **2001**, *113*, 2162 – 2163; d) J. I. Steinfeld, J. Wormhoudt, *Annu. Rev. Phys. Chem.* **1998**, *49*, 203 – 232; e) S. J. Toal, W. C. Trogler, *J. Mater. Chem.* **2006**, *16*, 2871 – 2883;f) D. S. Moore, *Rev. Sci. Instrum.* **2004**, *75*, 2499 – 2512; g) Y. Zimmermann, J. A. C. Broekaert, *Anal. Bioanal. Chem.* **2005**, *383*, 998 – 1002; h) L. J. Soltzberg, A. Hagar, S. Kridaratikorn, A. Mattson, R. Newman, *J. Am. Soc. Mass Spectrom.* **2007**, *18*, 2001 – 2006.
[16] a) S. W. Thomas III, J. P. Amara, R. E. Bjork, T. M. Swager, *Chem. Commun.* **2005**, 4572 – 2555; b) S. W. Thomas, III, G. D. Joy, T. M. Swager, *Chem. Rev.* **2007**, *107*, 1339 – 1386; c) K. K. Kartha, S. S. Babu, S. Srinivasan, A. Ajayghosh, *J. Am. Chem. Soc.* **2012**, *134*, 4834 – 4841; d) S. Zhang, F. Lu, L. Gao, L. Ding, Y. Fang, *Langmuir* **2007**, *23*, 1584 – 1590; e) H. Cavaye, P. E. Shaw, X. Wang, P. L. Burn, S.-C. Lu, P. Meredith, *Macromolecules* **2010**, *43*, 10253 – 10261; f) D. A. Olley, E. J. Wren, G. Vamvounis, M. J. Fernee, X. Wang, P. L. Burn, P. Meredith, P. E. Shaw, *Chem. Mater.* **2011**, *23*, 789 – 794.
[17] a) V. Vajpayee, H. Kim, A. Mishra, P. S. Mukherjee, P. J. Stang, M. Lee, H. K. Kim, K. W. Chi, *Dalton Trans.* **2011**, *40*, 3112 – 3115; b) S. Pramanik, C. Zheng, X. Zhang, T. J. Emge, J. Li, *J. Am. Chem. Soc.* **2011**, *133*, 4153 – 4155; c) S. Barman, J. A. Garg, O. Blacque, K. Venkatesan, H. Berke, *Chem. Commun.* **2012**, *48*, 11127 – 11129; d) K. Sarkar, Y. Salinas, I. Campos, R. Martínez-Máñez, M. D. Marcos, F. Sancenón, P. Amorós, *ChemPlusChem* **2013**, *78*, 684 – 694; e) Z. Hu, B. J. Deibert, J. Li, *Chem. Soc. Rev.* **2014**, *43*, 5815.
[18] a) H. H. Zeng, K. M. Wang, R. Q. Yu, *Anal. Chim. Acta* **1994**, *298*, 271 – 277; b) Y. Peng, A. J. Zhang, M. Dong, Y. W. Wang, *Chem. Commun.* **2011**, *47*, 4505 – 4507; c) G. He, H. Peng, T. Liu, M. Yang, Y. Zhangand, Y. Fang, *J. Mater. Chem.* **2009**, *19*, 7347 – 7353; d) B. Gole, S. Shanmugaraju, A. K. Bar, P. S. Mukherjee, *Chem. Commun.* **2011**, *47*, 10046 – 10048; e) D.-S. Kim, M. Lynch, K. A. Nielson, C. Johnsen, J. O. Jeppesen, J. L. Sessler, *Anal. Bioanal. Chem.* **2009**, *395*, 393 – 400; f) S. Shanmugaraju, S. A. Joshi, P. S. Mukherjee, *Inorg. Chem.* **2011**, *50*, 11736 – 11745.
[19] M. Alfonso, A. Sola, A. Caballero, A. Tárraga, P. Molina, *Dalton Trans.* **2009**, 9653 – 9658.
[20] The recognition properties were investigated in the presence of the following sets of metal cations and anions. a) metal cations: Li^+, K^+, Mg^{2+}, Cd^{2+}, Ni^{2+} and Pb^{2+} used as their perchlorate salts, and Na^+, Ca^{2+}, Cu^{2+}, Zn^{2+}, and Hg^{2+} as their triflate salts; b) anions: F^-, Cl^-, Br^-,I^-, $H_2PO_4^-$, $HP_2O_7^{3-}$, HSO_4^-, CN^-, AcO^-, PF_6^-, BF_4^-, ClO_4^-, NO_3^- and OH^- used as their tetrabutyl ammonium salts.
[21] The titration experiments were analyzed using the computer program Specfit (v.3.0.36 for 32-bit Windows) (Specfit/32 Global Analysis System, 1999 – 2004 Spectrum Software Associates (SpecSoft@compuserve.com)). This program was acquired from Bio-logic, SA (www.bio-logic.info) in January 2005. The equation to be adjusted by nonlinear regression, using the above mentioned software, was the following: $\Delta A/b = \{K_{11}\Delta\varepsilon_{HG}[H]_{tot}[G]\}/\{1\ K_{11}[G]\}$, where H = host, G = guest, HG = complex, ΔA = variation in the absorption, b = cell width, K_{11} = association constant for a 1:1 model, and $\Delta\varepsilon_{HG}$ = variation of molar absorptivity.
[22] M. Shortreed, R. Kopelman, M. Kuhn, B. Hoyland, *Anal. Chem.* **1996**, *68*, 1414 – 1418.
[23] P. D. Beer, A. R. Graydon, A. O. M. Johnson, D. K. Smith, *Inorg. Chem.* **1997**, *36*, 2112 – 2118.
[24] NCIplot, version 1.1., Department of Chemistry, Duke University, Durham (USA), **2011**; Homepage: http://www.chem.duke.edu/~yang/Software/software NCI.html; References: E. R. Johnson, S. Keinan, P. Mori-Sánchez, J. Contreras García, A. J. Cohen, W. Yang, *J. Am. Chem. Soc.* **2010**, *132*, 6498 – 6506; J. Contreras-García, E. R. Johnson, S. Keinan, R. Chaudret, J.-P. Piquemal, D. N. Beratan, W. Yang, *J. Chem. Theory Comput.* **2011**, *7*, 625 – 632.
[25] Here, λ_2 stands for the second highest eigenvalue of the electron density Hessian matrix. Based on electron density and its derivatives, the resulting figure highlights real space regions with electron density regimes below that of typical covalent bonds and ranging from strong or moderate noncovalent interactions (NCIs) (e.g., hydrogen bonds), weak interactions (e.g., van der Waals interactions) and steric (repulsive) clashes. (See Supporting Information for a more detailed description.) Some of the interactions belonging to the important van der Waals category display very weak bond strength. For instance, the methane dimer computed at B3LYP-D3/def2-SVP (gas phase) features d_{C-C} = 3.715 Å, $\rho(r) = 0.24\times10^{-2}\ e/a_o^3$ as previously reported: V. Nesterov, A. Espinosa, G. Schnakenburg, R. Streubel, *Chem. Eur. J.* **2014**, *20*, 7010 – 7016.
[26] The fluorescence quantum yields were measured with respect to anthracene as standard ($\Phi = 0.27$). W. R. Dawson, M. W. Windsor, *J. Phys. Chem.* **1968**, *72*, 3251 – 3260.
[27] ORCA – An ab initio, DFT and semiempirical SCF-MO package, version 3.0.2., Max Planck Institute for Bioinorganic Chemistry, Mülheim an der Ruhr (Germany), **2012**; Homepage: http://www.cec.mpg.de/forum/portal.php; Reference: F. Neese, *WIREs Comput. Mol. Sci.* **2012**, *2*, 73 – 78.
[28] Y. Zhao, D. G. Truhlar, *Theor. Chem. Acc.* **2008**, *120*, 215 – 241.
[29] a) A. Schäfer, C. Huber, R. Ahlrichs, *J. Chem. Phys.* **1994**, *100*, 5829 – 5835; b) F. Weigend, R. Ahlrichs, *Phys. Chem. Chem. Phys.* **2005**, *7*, 3297 – 3305.
[30] F. Neese, F. Wennmohs, A. Hansen, U. Becker, *Chem. Phys.* **2009**, *356*, 98 – 109.
[31] a) A. Klamt, G. Schüürmann, *J. Chem. Soc. Perkin Trans. 2* **1993**, 799 – 805; b) A. Klamt, *J. Phys. Chem.* **1995**, *99*, 2224 – 2235.
[32] A. Bergner, M. Dolg, W. Kuchle, H. Stoll, H. Preuss, *Mol. Phys.* **1993**, *80*, 1431 – 1441. Obtained from the EMSL Basis Set Library at https://bse.pnl.gov/bse/portal. D. Feller, *J. Comput. Chem.* **1996**, *17*, 1571 – 1586.
[33] C. Riplinger, B. Sandhoefer, A. Hansen, F. Neese, *J. Chem. Phys.* **2013**, *139*, 134101.
[34] a) L. Goerigk, S. Grimme, *J. Chem. Theory Comput.* **2011**, *7*, 291 – 309; b) L. Goerigk, S. Grimme, *Phys. Chem. Chem. Phys.* **2011**, *13*, 6670 – 6688.
[35] S. Grimme, J. Antony, S. Ehrlich, H. Krieg, *J. Chem. Phys.* **2010**, *132*, 154104 – 154119.
[36] a) S. Grimme, *J. Chem. Phys.* **2003**, *118*, 9095 – 9102; b) S. Grimme, L. Goerigk, F. F. Reinhold, *WIREs Comput. Mol. Sci.* **2012**, *2*, 886 – 906.
[37] a) F. Neese, F. Wennmohs, A. Hansen, *J. Chem. Phys.* **2009**, *130*, 114108; b) F. Neese, A. Hansen, F. Wennmohs, S. Grimme, *Acc. Chem. Res.* **2009**, *42*, 641 – 648.
[38] F. Wennmohs, F. Neese, *Chem. Phys.* **2008**, *343*, 217 – 230.
[39] NBO 5.0 code, E. D. Glendening, J. K. Badenhoop, A. E. Reed, J. E. Carpenter, J. A. Bohmann, C. M. Morales, F. Weinhold, Theoretical Chemistry Institute, University of Wisconsin, Madison, **2001**.
[40] a) P.-O. Löwdin, *J. Chem. Phys.* **1950**, *18*, 365 – 375; b) P.-O. Löwdin, *Adv. Quantum Chem.* **1970**, *5*, 185 – 199; c) A. Szabo, N. S. Ostlund, *Modern Quantum Chemistry. Introduction to Advanced Electronic Structure Theory*, Dover Publications, Mineola, NewYork, **1989**.
[41] R. F. W. Bader, *Atoms in Molecules: A Quantum Theory*, Oxford University Press, Oxford, **1990**.
[42] AIM2000, version 2.0., Fachhochschule Bielefeld (Germany), **2002**; Homepage: http://www.aim2000.de/; References: F. Biegler-König, J. Schönbohm, D. Bayles, *J. Comput. Chem.* **2001**, *22*, 545 – 559; F. Biegler-König, J. Schönbohm, *J. Comput. Chem.* **2002**, *23*, 1489 – 1494.
[43] VMD – Visual Molecular Dynamics (v.1.9.1), Theoretical and Computational Biophysics Group, University of Illinois at Urbana-Champaign (USA), 2012; Homepage: http://www.ks.uiuc.edu/Research/vmd/; W. Humphrey, A. Dalke, K. Schulten, *J. Molec. Graphics* **1996**, *14*, 33 – 38.

Received: July 9, 2014
Published online on September 26, 2014